ACS OMEGA

Open Access

http://pubs.acs.org/journal/acsodf

Article

Carbonic Anhydrase Robustness for Use in Nanoscale CO_2 Capture Technologies

Arjun Sharma,[#] Rong-an Chiang,[#] Monica Manginell, Isaac Nardi, Eric N. Coker, Juan M. Vanegas, Susan B. Rempe,* and George D. Bachand*

Cite This: *ACS Omega* 2023, 8, 37830−37841

Read Online

ACCESS | Metrics & More | Article Recommendations

ABSTRACT: Continued dependence on crude oil and natural gas resources for fossil fuels has caused global atmospheric carbon dioxide (CO_2) emissions to increase to record-setting proportions. There is an urgent need for efficient and inexpensive carbon sequestration systems to mitigate large-scale emissions of CO_2 from industrial flue gas. Carbonic anhydrase (CA) has shown high potential for enhanced CO_2 capture applications compared to conventional absorption-based methods currently utilized in various industrial settings. This study aims to understand structural aspects that contribute to the stability of CA enzymes critical for their applications in industrial processes, which require the ability to withstand conditions different from those in their native environments. Here, we evaluated the thermostability and enzyme activity of mesophilic and thermophilic CA variants at different temperature conditions and in the presence of atmospheric gas pollutants like nitrogen oxides and sulfur oxides. Based on our enzyme activity assays and molecular dynamics simulations, we see increased conformational stability and CA activity levels in thermostable CA variants incubated week-long at different temperature conditions. The thermostable CA variants also retained high levels of CA activity despite changes in solution pH due to increasing NO and SO_2 concentrations. A loss of CA activity was observed only at high concentrations of NO/SO_2 that possibly can be minimized with the appropriate buffered solutions.

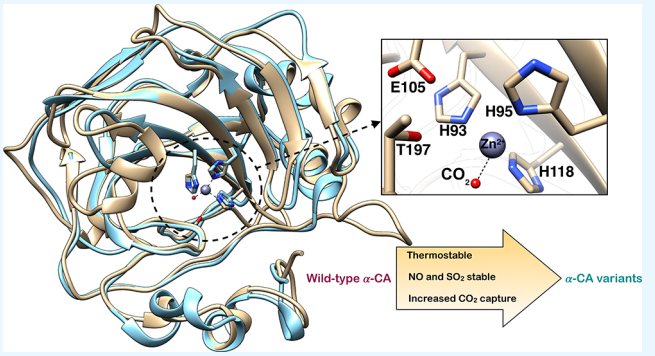

1. INTRODUCTION

Carbon dioxide (CO_2) is one of the main anthropogenic greenhouse gases and a significant contributor to the increasing average global temperature.[1−3] There is a strong correlation between a surge in CO_2 levels in the atmosphere and an increase in temperature.[4] This increase in CO_2 levels affects the earth's surface temperature, as currently evidenced by the melting of polar ice caps in the Arctic Circle and Antarctic ice sheets, contributing to rising sea levels and ocean acidity.[5−7] Human-induced activities, such as fossil fuel burning and deforestation, are the primary reasons for elevated atmospheric CO_2 levels. Fossil fuel combustion accounts for nearly 75% of total CO_2 emissions.[8] Conventional fossil fuel-fired power plants emit flue gas that is released into the atmosphere without removing CO_2 and other pollutant gases, including nitrogen oxides (NO_x) and sulfur oxides (SO_x), that adversely affect the ozone layer. According to a recent report by the International Energy Agency (IEA), carbon capture and storage systems (CCS) could reduce the annual CO_2 emissions by as much as 6 gigatonnes by 2050. This amount accounts for a 14% decrease in total carbon emission, which is necessary to limit the global temperature increase to 2 °C by the end of the 21st century.[9] To achieve this ambitious goal, it is important to develop inexpensive materials that can capture CO_2 cost-effectively and be regenerated with minimal energy consumption.

The benchmark CO_2 capture methodologies for post-combustion capture (PCC), such as amine solvent-based technology, use liquid absorption. In that process, an aqueous amine sorbent in a gas absorption column reacts with CO_2 in a gas to form a mixture of carbamate and bicarbonate species.[10,11] The CO_2-rich amine is then transferred to a stripping column, where it is steam-heated to 100−140 °C to release the CO_2 and regenerate the amine sorbent. The main advantage of this methodology is its high absorption rate and high selectivity for CO_2 relative to those of other conventional alternatives. Another advantage is that it can be retrofitted into

Received: April 17, 2023
Accepted: September 8, 2023
Published: October 5, 2023

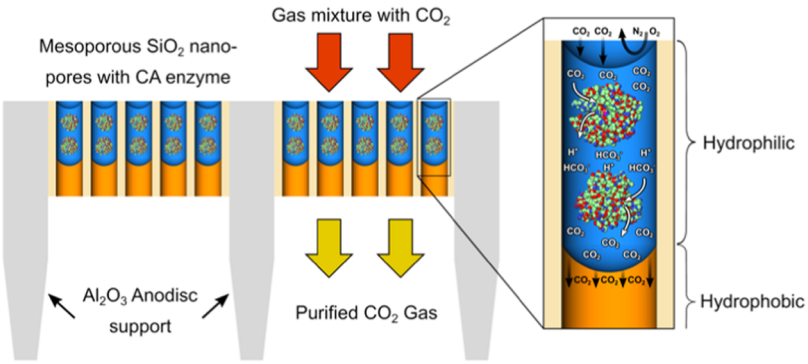

Figure 1. Schematic representation of ultrathin mesoporous silica (SiO_2) membrane layer containing CA enzymes in aqueous solution embedded within thick alumina (Al_2O_3) Anodisc column supports. The silica mesopores are functionalized to be hydrophobic, except for the first few nanometers from the pore surface, which is hydrophilic. This unique liquid membrane framework maximizes CO_2 solubilization and conversion into bicarbonate ion (HCO_3^-) at the hydrophilic upstream surface, and regeneration of CO_2 at the hydrophobic downstream surface[31] for storage. This material motivates the current work.

existing power and industrial plants. However, there are several disadvantages to using amine-based CO_2 capture solvents; mainly, the costs associated with the application of a technology that increases the energy consumption of a power plant by an estimated 25−40%,[12] thus limiting its widespread use. The high heat capacity of water and the substantial water vaporization that is needed for the stripping step make the process energy-intensive. Also, the basic amine solution is corrosive and can damage the capture equipment with prolonged use. The volatility and susceptibility of amine absorbent to evaporation and chemical degradation lead to amine loss over time. This amine loss during the CO_2 capture process generates toxic aerosols and wastes that can harm the environment.

As an alternative, Fradette et al.[13] developed a proprietary enzyme-catalyzed solvent technology to replace conventional amine-based solvents for PCC applications, with CO_2 capture rates between 65 and 95%. However, the enzyme stability performances were recorded at a specific temperature (60 °C) and without toxic industrial contaminants that could significantly hamper the CO_2 capture efficiency. A better understanding of the mechanisms that stabilize the enzyme structure under non-native conditions may be helpful in advancing this technology. Despite recent advances in existing PCC technologies, there is an urgent need to develop novel CCS technologies that are economically feasible, efficient, and environmentally friendly and that minimize the energy penalty for regeneration.

Membrane-based separation approaches have shown promising potential as the next-generation PCC technology.[14,15] Some advantages of membrane-based technologies are their relatively low cost, low energy consumption, flexible operation, and absence of corrosive and toxic materials, which make them environmentally friendly. In selecting membrane materials, key features include high CO_2 selectivity, high gas permeance, robustness under industrial operating conditions, and the ability to meet separation requirements.[16] Favre's recent review comprehensively summarizes the latest advancements in membrane separation technologies in postcombustion carbon capture applications.[17]

Conventional gas separation membranes are mostly made of thin-film polymer or composite materials,[18] which are usually limited by a trade-off in gas permeation rate and CO_2 selectivity, short lifetime, and lack of membrane stability as a result of continuous exposure to acid gas impurities, such as NO and SO_2.[19] Another primary limitation of membrane-based separation is the requirement for a large membrane area due to the low partial pressure of carbon dioxide in the flue gas,[20,21] which can increase the overall cost and complexity of the system. Additionally, gas membranes operate based on pressure differentials, leading to a notable pressure drop across the membrane. This pressure drop necessitates additional energy to maintain optimal gas flux and overcome back pressure, thereby impacting the overall energy consumption of the process.

Membrane material selection and operating temperatures also pose challenges in PCC.[22−24] The choice of the membrane material can affect the separation efficiency and energy requirements. Some materials may exhibit selectivity, permeability, or stability limitations, necessitating further research and development. Furthermore, operating temperatures can affect the membrane performance, requiring additional temperature control measures that may contribute to increased energy consumption. A technical report prepared for the U.S. Department of Energy estimated that CO_2 capture by a membrane would be feasible.[25] This report details the energy-intensive nature of membrane-carbon capture processes and economic considerations. However, it is important to note that membrane material development is an ongoing area of research. Rapid advances are being made in material development, module design, and process optimization to address the limitations and enhance the efficiency and cost-effectiveness of membrane-based separations in PCC.[26,27]

Several groups over the years have adopted strategies to improve CCS using biocatalytic gas−liquid membrane contactors for industrial applications.[28−30] In a recent breakthrough, Fu and colleagues introduced a liquid-layered biomimetic CO_2 separation membrane called the MemZyme technology. This innovation incorporates a naturally occurring enzyme, resulting in performance advantages over other alternatives when subjected to laboratory evaluations. The MemZyme membrane (Figure 1) consists of carbonic anhydrase (CA) enzymes embedded within an ultrathin (of order 0.1 nm) layer of nanoporous silica membrane and has shown considerable promise as enzyme-enhanced CCS.[31] MemZyme technology stands out due to its unmatched combined selectivity for CO_2 over N_2 and high CO_2 permeance, making it a promising solution to CCS. This

https://doi.org/10.1021/acsomega.3c02630
ACS Omega 2023, 8, 37830−37841

enzymatic liquid membrane motivates the current studies of CA enzymes.

CAs are mostly zinc metalloenzymes and found ubiquitously in Nature, being present in prokaryotes, eukaryotes, and extremophiles.[32−34] There are five distinct classes of CA enzyme families that are evolutionarily unrelated;[32] namely, α, β, γ, δ, and ζ. These different classes of CA share low sequence similarities and have different secondary structure folds. However, all CA classes use the same catalytic mechanism, involving the reversible hydration/dehydration of CO_2 into bicarbonate and a proton, as shown below (eqs 1, 2, and 3).[35]

$$(Zn^{2+} - H_2O) \rightleftharpoons (Zn^{2+} - OH^-) + H^+ \quad (1)$$

$$(Zn^{2+} - OH^-) + CO_2 \rightleftharpoons (Zn^{2+} - HCO_3^-) \quad (2)$$

$$(Zn^{2+} - HCO_3^-) + H_2O \rightleftharpoons (Zn^{2+} - H_2O) + HCO_3^- \quad (3)$$

The active site of the CA enzyme involves a zinc ion (Zn^{2+}) coordinated with three histidine side chains and a water molecule, which acts as a fourth coordination site. In the mechanism above, protons are transferred from the Zn^{2+}-bound water molecule (Zn^{2+}−H_2O) to a fourth histidine and then to the bulk solvent, forming a highly ordered hydrogen-bonded network to facilitate proton shuttle[34] and generate a negatively charged Zn^{2+}−OH^- hydroxide ion. The electrostatic interactions in the active site contribute to the pK_a of catalytic residues during the reaction.[36] At the same time, the weak hydration free energy of the CO_2[37] is responsible for the transport of the small molecule in and out of the active site.[36,37] Once CO_2 reaches the active site, it binds to Zn^{2+}−OH^- and is converted to HCO_3^- through a nucleophilic attack. An internal proton transfer forms Zn^{2+}−HCO_3^-, which then binds to H_2O, resulting in Zn^{2+}−H_2O reformation. Simultaneously, HCO_3^- is released into the solvent. This highly efficient CA enzymatic mechanism can tackle large-scale CO_2 emissions from industries as CAs are known for their high turnover rates, up to 1×10^6 s^{-1}, making them one of the fastest catalysts in Nature.

One of the main challenges in the large-scale implementation of enzymes for industrial applications is the protein catalyst's thermochemical stability to harsh operating conditions such as constant exposure to elevated temperature and acid gas contaminants. To address this challenge, several research groups have isolated CAs from thermophiles and immobilized CA enzymes on solid support substrates.[28,38−46] The other enzyme management concerns include, but are not limited to, absorption kinetics over time and the potential recovery and reusing of enzymes.

In this work, we investigated CAs suitable for industrial-scale CCS applications for their thermal stability and catalytic efficiency under different temperature conditions and in the presence of gas and acid contaminants using experimental and computational methods. Although earlier studies have investigated the thermal stability of CAs,[47−53] comparative studies of mesophilic and thermophilic CAs are scarce,[54,55] particularly involving exposure to high-temperature conditions and industrial contaminants like NO and SO_2 toxic gases.[56] Our study is aimed at gaining insights into the structural elements in CAs that impart stability in solution against high temperatures and industrial contaminants. These data establish a baseline assessment for subsequent studies focused on using CA within the confines of membrane nanopores (Figure 1) to enhance the enzymatic performance in CCS applications.

2. MATERIALS AND METHODS

2.1. Carbonic Anhydrase (CA) Enzymes. Bovine carbonic anhydrase (BCA) was purchased from Worthington Biochemical Corporation as a dry powder, and stock solutions (150 μM) were prepared either in deionized (DI) water or 12.5 mM Tris buffer (pH 7.5) and 75 mM NaCl. A proprietary CA variant (XCA) was supplied by Novozymes and prepared in 12.5 mM Tris buffer (pH 7.5) and 75 mM NaCl. Three recombinant variants of CA from *Persephonella marina* EX-H1were supplied by EpigenTor Consultants, Inc.: wild-type PmCA (WT), and two genetically engineered variants, PmCA (WW) and PmCA (SC).

The coding sequence for PmCA (WT) from the NCBI database (accession code WP_015898908) was synthesized by Biomatik, Inc., including codon optimization for expression in *E. coli*. The PmCA gene was cloned into plasmid pET22b at sites 5′ NdeI and 3′ *Hin*dIII by restriction digest and ligation, which imparted a C-terminal 6X Histidine tag on the recombinant protein. Variants PmCA (WW) and PmCA (SC) were generated using the Q5 Site-Directed Mutagenesis Kit (New England Biolabs). All plasmids were transformed into Rosetta 2 chemically competent *E. coli* bacteria, and a single colony was selected and grown in a 25 mL culture overnight at 37 °C and 240 rpm in Terrific Broth (TB) supplemented with 1% glucose and 0.8% glycerol with 100 μg/mL carbenicillin and 34 μg/mL chloramphenicol. To the overnight culture was added 1 L of the supplemented TB broth, and the culture was grown to an $OD_{600\ nm}$ of 0.4−0.8, at which point ITPG (isopropyl β-D-1-thiogalactopyranoside) was added to a concentration of 0.4 mM to induce protein expression. The temperature at induction was reduced to 30 °C, and the culture was incubated with shaking (240 rpm) for 10 h. Cells were then harvested by centrifugation, and bacterial pellets were resuspended in 5.5× PBS (phosphate-buffered saline: 753.5 mM NaCl, 14.85 mM KCl, 55 mM Na_2HPO_4, and 9.9 mM KH_2PO_4, pH 7.4) supplemented with Roche Protease inhibitors, 1 mM PMSF (phenylmethylsulfonyl fluoride), 10% glycerol, 0.15% Triton-X, and 15 mM imidazole. Cells were lysed with sonication on ice (4 cycles, 45 s on, followed by 2 min rests). Lysates were centrifuged at 4 °C for 20 min at 12,000*g*, and the supernatant was incubated with N-NTA agarose at 4 °C for 3 h. The beads were washed with 2 column volumes of 5.5× PBS supplemented with 0.15% Triton-X, and 30 mM imidazole, and then eluted with 5.5× PBS supplemented with 300 mM imidazole.

2.2. PmCA Variants. We designed a library of PmCA variants, of which we picked PmCA (SC) and PmCA (WW). PmCA (SC) has negatively charged mutations on the outer shell of the enzyme, giving it an overall net negative charge (see the Results section). These mutations were made to give the enzyme tolerance against acidic pH as the more CO_2 that is harvested, the lower the pH becomes with the buildup of carbonic acid. Negatively charged proteins generally are more tolerant of an acidic pH.[57,58] The PmCA (WW) variant contains mutations within the enzyme's active site that were aimed at increasing proton transfer and hydration to carbon dioxide (see the Results section). CO_2 hydration, catalyzed by CA enzymes, is a critical rate-limiting step in the conversion process of carbon dioxide to bicarbonate.[59−61]

https://doi.org/10.1021/acsomega.3c02630
ACS Omega 2023, 8, 37830−37841

2.3. CA Esterase Activity Assay. CA catalyzes the hydration of CO_2 to bicarbonate, but the active site also displays esterase activity with a variety of different ester types.[62] Further, measuring the esterase activity serves as an effective surrogate to characterize changes in CA activity.[52,63,64] The reaction involves the hydrolysis of p-nitrophenyl acetate (pNPA) to produce p-nitrophenol (pNP), which can be measured by absorption spectroscopy at 405 nm (A405) using a UV/vis 96-well plate reader. Briefly, 200 μL reactions were prepared in 96-well plates by adding CA samples to assay buffer (12.5 mM Tris buffer (pH 7.5) and 75 mM NaCl) containing 1 mM pNPA, and placing the 96-well plate into the plate reader (PerkinElmer Victor 3). A standard dilution curve of pNP (0−1000 μM) was included on all plates to convert the A405 measurements to pNP concentration in μM. A405 measurements were recorded at regular intervals (e.g., 3 min) for 1−2 h. All reactions were performed at ambient temperature (23 °C) and with a concentration of 12 μM CA. Standard curves were analyzed using regression analysis (SigmaPlot), and A405 measurements were converted to pNP concentrations for all samples. Regression analysis (concentration vs time) was then used to determine the CA reaction velocity (V) in μM/min. This value (V) was then converted to specific activity A_{CA} (min^{-1}) by dividing by the concentration of CA (i.e., 12 μM):

$$A_{CA} = \frac{V}{[CA]} \quad (4)$$

2.4. Temperature, Gas, and Acid Effects. *2.4.1. Temperature Effects on CA Activity.* The temperature stability of BCA and PmCA variants was evaluated by storing samples of enzymes at either 4 or 70 °C. Samples were selected randomly at Days 0, 3, and 7, and the esterase activity was measured, as described above. The retention of activity was determined by dividing the activity at Day 3 or 7 by that observed at Day 0. It should be noted that the esterase activity was measured after samples were removed from the defined storage temperature and equilibrated to 23 °C. The percent remaining activity was calculated by dividing the activity (A_{CA}) at a given time point by the initial activity (t = 0).

2.4.2. Impact of Contaminating Gas on CA Activity. The impact of the gas content on the activity of the different CA enzymes was examined by exposing aliquots of the enzyme in bulk solution to flowing gas for 4 h. All gases were purchased from Matheson Trigas and used as received (CO_2, UHP grade; H_2S, 2% in N_2 UHP grade; propane, UHP grade; NO 1513 ppm + SO_2 505.2 ppm + CO_2 5.019% + N_2 balance, CALMAT-1 grade). Specific gas mixtures were achieved by blending two or more gas streams using mass flow controllers (Brooks Instruments), which were calibrated for each specific gas using a bubble meter at known temperatures and pressure. The exposures were conducted in a plastic chamber (saturator) with gas inlet and outlet ports, and an O-ring seal between base and lid (Figure 2). Each experiment was run at room temperature under a set total gas flow rate of 200 ± 5 sccm (mL/min at STP). A reservoir of deionized water was added into the base of the saturator to provide a level of humidity (the dew point of the gas phase over the samples was 25 ± 1 °C) that would reduce evaporation from the enzyme solutions during the test. The mass of each sample was measured prior to and after gas exposure and suggested negligible evaporative loss for all samples. Prior to each test, gas flow was established, and the stability of the mass flow controller output was verified.

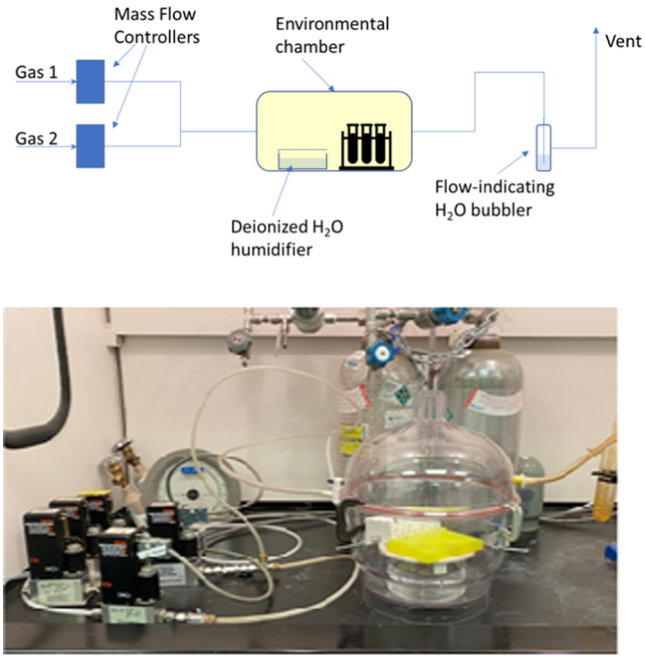

Figure 2. (Top) Schematic and (bottom) photograph of the experimental setup used to expose CA enzymes to various mixtures of gases.

The outlet from the saturator was connected to a water bubbler to visualize positive flow and provide a minimal overpressure of gas to mitigate any ingress of air through the saturator's O-ring seal. Enzyme samples were loaded into the saturator and exposed to the desired gas for 4 h, after which the solutions were removed from the saturator and sealed immediately, and CA activity was measured. The retention in esterase activity was determined by dividing the activity at t = 4 h by that observed prior to exposure (i.e., t = 0 h).

2.4.3. Effect of Nitric and Sulfuric Acids on CA Activity. To characterize the effects related to pH, aliquots of BCA and PmCA were exposed to HNO_3 or H_2SO_4, with concentrations ranging from 1 to 50 mM. Concentrated HNO_3 or H_2SO_4 acids were diluted in either Tris (BCA) or 5.5× PBS (PmCA) and the pH was measured. Stock CA solutions were then diluted to 12 μM in these acid-containing solutions. To differentiate pH versus anion effects, the activity of BCA was also characterized by exposing samples of the enzyme to solutions containing 1−50 mM HNO_3 or H_2SO_4, where the pH was adjusted to ∼7.4 using the addition of NaOH. The esterase activity was measured as described above, and the relative activity was determined by dividing the CA activity for a given concentration by activity observed for samples containing 1 mM of acid, which was shown in initial experiments to have little to no effect on activity.

2.5. Molecular Dynamics Simulations. The native structure of α-type carbonic anhydrases from BCA (PDB code: 1V9E) and PmCA (PDB code: 6IM1) were obtained from the RCSB protein data bank. All molecular dynamics (MD) simulations were performed using the GROMACS simulation package v2019.[65] Protein residues were modeled using the AMBER 99SB-ILDN force field in combination with the specialized zinc metal ion and coordinating amino acid residues' (HIS/GLU) parameters developed by Procacci and co-workers.[66−69] The TIP3p model[70] was used for water. The pK_a of the amino acid side chain residues at neutral pH 7.0

https://doi.org/10.1021/acsomega.3c02630
ACS Omega 2023, 8, 37830−37841

were determined using PROPKA3.[71,72] The GLU residue in BCA (103) and PmCA (113) was modified to GLUH to represent the correct protonation state using the GROMACS pdb2gmx command. Only one monomer from the homodimer PmCA structure was selected for MD simulations.

To investigate the thermal stability of protein configurations, a set of systems at four different temperatures were modeled for both BCA and PmCA. The simulations were carried out at 25, 70, 100, and 140 °C temperatures. For all systems, the protein structure was centered in a 9 nm^3 cuboid water box with a minimum distance of 1 nm between the protein structure and the box boundaries. The appropriate number of counterions [sodium (Na^+) or chlorine (Cl^-)] were added to electroneutralize the charge of the solvated systems. Long-range electrostatic interactions were calculated using the particle-mesh Ewald (PME)[73] with a grid size of 0.12 nm and a real-space radius of 1.6 nm. A nonbonded cutoff of 1.6 nm was used for the Lennard-Jones potential. The LINCS algorithm[74] was used to constrain all hydrogen bonds. The steepest descent method was applied for 500 cycles to perform energy minimization. A stochastic velocity-rescaling thermostat[75] and stochastic cell-rescaling barostat[76] were used to keep the system at specified temperatures and 1 atm, with coupling times of 1 and 5 ps, respectively. The periodic boundary conditions were set to all three box dimensions. The integration time step was 2 fs for MD simulations, and data were collected every 5 ps. The Maxwell−Boltzmann distribution was applied to generate initial velocities for systems at different temperatures. The systems were allowed to equilibrate at specified temperatures in an isothermal−isobaric (NPT) ensemble for 100 ns before 1 μs of production MD simulation for data collection. The analyses were performed on the final 200 ns of simulation trajectories.

Chimera 1.15[77] and VMD 1.9.2[78] were used for the visualization of protein structural representations from MD simulations. The GROMACS embedded tools were utilized to compute the root-mean-square deviation (RMSD) and evaluate the structural stability of the protein backbone. The dictionary of secondary structures of proteins (DSSP) algorithm[79] was used to characterize protein dynamics in solution.

3. RESULTS AND DISCUSSION

3.1. Temperature Dependence. Temperature stability is a key requirement for many applications involving CA; in particular, elevated temperatures (>60 °C) are commonly used for CCS processes.[52,80] A key element in the use of CA in carbon capture technology is the ability of the enzyme to remain stable and function over time at elevated temperatures. Thus, we characterized the activity of different CA variants maintained at 4 or 70 °C for 7 days.

BCA, in either water or Tris buffer, maintained 79% of its initial activity when kept at 4 °C for 7 days, which contrasts with the complete loss of activity observed at Days 3 and 7 when maintained at 70 °C (Figure 3). This observation is consistent with prior reports suggesting that BCA activity is lost at temperatures exceeding 60 °C.[81,82] It should be noted that the percent of remaining activity exceeded 100% in some cases and may be attributed to the intrinsic variation in the esterase activity.

A similar decrease in activity (i.e., ∼58% activity retention over 7 days) was observed for the PmCA variants stored at 4 °C (Figure 3A). These variants, however, displayed a much

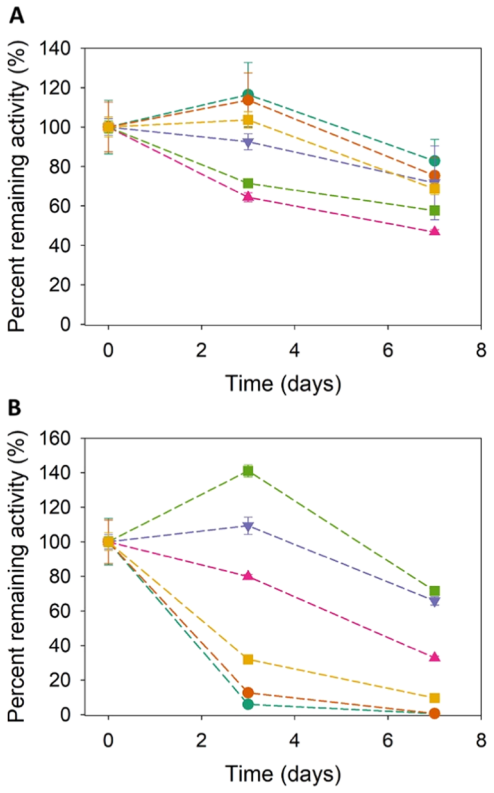

Figure 3. Remaining activity of carbonic anhydrase (CA) samples following storage for 7 days at (A) 4 °C or (B) 70 °C. Enzymes tested were: BCA (DI) (green -●-), BCA (Tris) (orange -●-), PmCA (WT) (purple -▼-), PmCA (WW) (pink -▲-), PmCA (SC) (green -■-), and XCA (gold -■-). Error bars equal the propagated standard error of the mean.

greater level of activity retention when maintained at 70 °C (Figure 3B), compared to BCA, with an average remaining activity of 57% at Day 7. PmCA (WW) displayed a lower level of stability at 70 °C compared with PmCA (WT), which can be attributed to the mutations in the active site (Figure 4A). The mutations in PmCA affected the electrostatic potential of the PmCA active site and lowered the thermal stability of the enzyme. In contrast, the PmCA (SC) performed as well or better than the wild-type PmCA, retaining >70% of the initial activity at Day 7. Here, the mutations altered the electrostatic potential of the outer shell of the enzyme, rendering it more negative (Figure 4B), while maintaining/enhancing the temporal stability of PmCA (SC) at 70 °C compared to the PmCA (WT). Qualitatively, these results for the PmCA variants agree with those reported for CAs from *P. marina* incubated at elevated temperatures over a shorter time frame.[54,63] Reports suggest that this thermostability may extend to temperatures as high as 100 °C, where a half-life of 88 min was reported for that temperature.[52]

3.2. Modeling of BCA and Wild-Type PmCA. Visual inspection of the superimposed crystal forms of BCA and PmCA (WT) reveals strong similarities in structural alignment (Figure 5). The zoomed-in portion shows a catalytic zinc ion in the central active site coordinated by three highly conserved histidine residues (His93, His95, and His118 in BCA) and a fourth ligand, which can be a water molecule or a hydroxide or bicarbonate anion. The catalytically relevant residues in BCA, namely, Glu105 and Thr197, are shown as well.

https://doi.org/10.1021/acsomega.3c02630
ACS Omega 2023, 8, 37830−37841

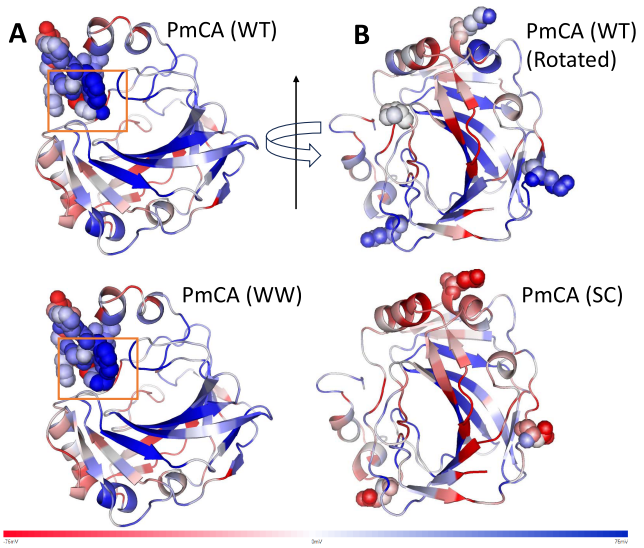

Figure 4. PmCA enzymes in two orientations (A, B) to highlight electrostatic differences between wild-type (WT) and variants WW and SC. (A) The electrostatic charge of the active site compared between PmCA (WT) and PmCA (WW). The orange box represents an amino acid residue change that modifies the electrostatic potential in the active site. (B) The electrostatic charge of the outer shell compared between PmCA (WT) and PmCA (SC). Spheres represent amino acid residue changes. These changes modify the electrostatic potential of the outer shell between the WT and the SC variant.

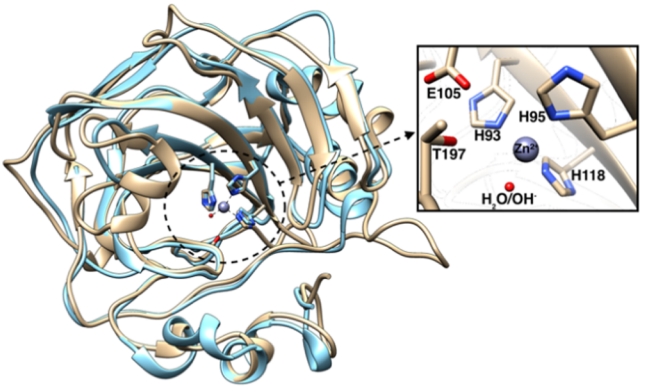

Figure 5. Ribbon representation of the superimposed configurations of BCA (tan) and PmCA (blue). The zoomed-in view of the active site of BCA shows the conserved residues along with the Zn^{2+} ion (purple sphere) and the H_2O/OH^- molecule (red sphere).

MD simulations were performed to investigate the differences in the thermal stability between BCA and PmCA (WT) at different temperatures. The global RMSD (root-mean-square deviation of the protein backbone from the starting configuration) analysis shows combined domain effects that affect the structural stability of the protein compared with the initial conformation. BCA is stable at a low temperature (25 °C), with an average RMSD value of 0.2 nm. The RMSD at 70 °C shows a steady increase until 380 ns, followed by a large shift and stabilization around 0.5 nm. This large shift in RMSD value close to 70 °C correlates with thermal denaturation of secondary and tertiary structures of BCA, as observed by Sarraf and co-workers in their UV/vis and CD spectrophotometric experiments.[83] The RMSD is relatively unstable at 140 °C, with significant fluctuations throughout the simulation time (Figure 6A). Comparatively, the RMSD for PmCA is stable at

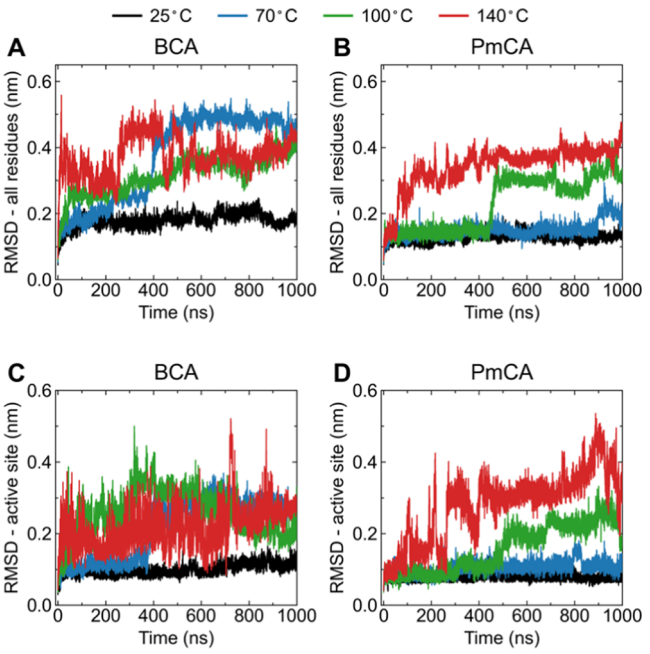

Figure 6. Molecular dynamics simulation results for BCA and PmCA at different temperature conditions. (A) RMSD of BCA and (B) PmCA main-chain backbone. Both BCA and PmCA show an average RMSD value of less than 0.5 nm for all isotherm simulations, indicating the thermal stability of protein structure. RMSD of conserved residues that are part of the active site in (C) BCA (His93, His95, and His118 that coordinate with the central Zn^{2+} ion and the catalytically important residues Glu105 and Thr197), and (D) PmCA (His86, His88, and His105 that coordinate with the central Zn^{2+} ion and the catalytically important residues Glu92 and Thr172).

both 25 and 70 °C. A slight jump in the RMSD value from 0.15 to 0.3 nm was observed after 400 ns at 100 °C. The system at 140 °C sees a sharp increase within the first few nanoseconds and then stabilizes after 500 ns (Figure 6B). Based on this analysis, the PmCA has lower structural flexibility and thus higher thermal stability than BCA across different temperature systems.

The RMSD values were also calculated exclusively for the active site residues in BCA and PmCA. The results show that the RMSD in BCA is stable only at 25 °C, and all other high-temperature systems show large fluctuations throughout the simulation period (Figure 6C). The PmCA shows stable RMSD values at both 25 and 70 °C. The RMSD is relatively stable at 100 °C for the first 500 ns and subsequently increases to 0.28 nm by the end of the simulation. The system at 140 °C displays more continuous fluctuations at the RMSD (Figure 6D). A comparison of the average change in RMSD values between BCA and PmCA shows that PmCA is relatively more stable than BCA in high-temperature environments. This localized RMSD analysis provides us with a closer look at the flexibility of the CA catalytic core. That core is not coupled to global interdomain interactions. It participates directly in the two-step catalytic mechanism of CO_2 hydration involving proton transfer reactions to and from ordered water molecules.

The changes in protein secondary structures are important indicators to gauge its folding/unfolding process. We probed the percentage of α-helices over the course of our simulations to account for differences in conformational thermal stability between BCA and PmCA as a function of temperature.

https://doi.org/10.1021/acsomega.3c02630
ACS Omega 2023, 8, 37830−37841

Our DSSP analysis shows a substantial decrease in the number of α-helices in BCA, going from 25 to 70 °C, with a minor change between 70 and 100 °C. A large drop is observed at 140 °C in BCA. The PmCA, interestingly, only shows a small change in the α-helicity between 25 and 70 °C. The PmCA system at 100 °C shows some decrease; however, the α-helicity descends rapidly at 140 °C (Figure 7).

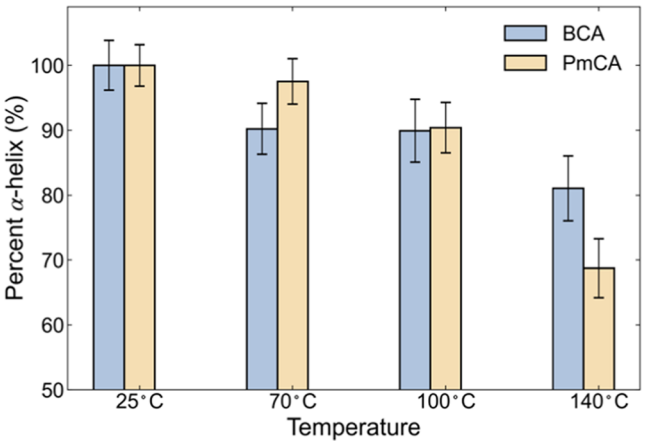

Figure 7. Secondary structure analysis using DSSP in BCA (blue) and PmCA (yellow) shows changing α-helicity at different temperatures from the last 200 ns of simulation time. Error bars equal one standard deviation of the mean.

To summarize, PmCA retains α-helicity across different temperatures, except for 140 °C. In contrast, BCA loses much of its α-helicity at 70 °C and continues to lose further at elevated temperatures. Given that α-helices are more robust to mutations compared to β-sheets,[71] the loss of α-helicity at higher temperatures (>60 °C) directly impacts the CA activity of BCA, as seen from our experiments (Figure 3A,B).

Intramolecular interactions such as hydrogen bonds are integral to a protein's secondary structures and conformational stability. In particular, the hydrogen bonds in the protein backbone confer rigidity and enhance the protein's thermal stability. The flexibility of a protein varies with the number of hydrogen bonds,[71] and protein structures become unstable at higher temperatures. Our hydrogen bonding analysis specifically examined the formation of hydrogen bonds between all potential donors and acceptors within a distance of 0.35 nm and an angle of 30°. We observed a substantial decline in the stability of BCA in relation to higher temperatures, from 170 hydrogen bonds at 25 °C to 158 at 140 °C (as depicted in Figure 8). In contrast, the PmCA structure demonstrated greater stability at elevated temperatures, exhibiting only a slight decrease in the total number of hydrogen bonds. At 25 °C, 147 hydrogen bonds, which decrease slightly to 141 at 140 °C (as illustrated in Figure 8). Notably, our hydrogen bonding analysis reinforced and validated our findings from the DSSP analysis.

3.3. Enzyme Activity and Contaminating Gases.

Industrial application of CA for CO_2 capture also necessitates stable enzyme activity in the presence of contaminating gas species such as NO_x (mainly NO) and SO_x (mainly SO_2).[56,84−86] To help achieve that goal, it is critical to understand the enzymatic performance of CA upon exposure to streams of various gases. Thus, we evaluated changes in enzyme activity after exposing solutions of the different CA

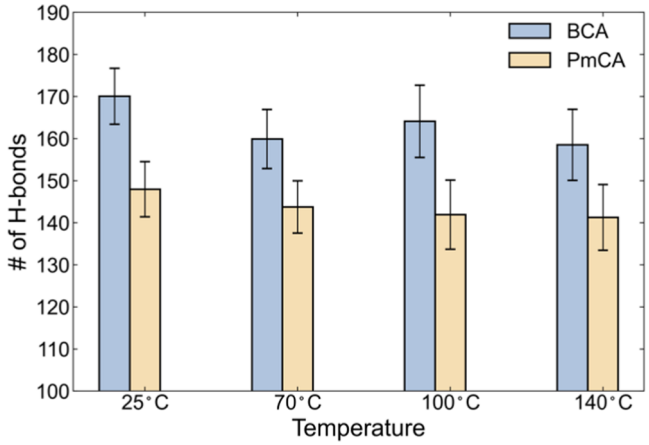

Figure 8. Hydrogen bond analysis for BCA (blue) and PmCA (yellow) at different temperatures from the last 200 ns of simulation time. Error bars equal one standard deviation of the mean.

variants for 4 h to gas mixtures containing N_2, CO_2, NO, SO_2, propane (C_3H_8), and hydrogen sulfide (H_2S). We anticipated that propane, an aqueous insoluble gas, would have no effect on CA activity, while the remaining soluble gases would potentially affect activity.

As expected, all of the six CA variants exposed to the control treatment, i.e., 15.3% CO_2 with a balance of N_2, displayed no changes in esterase activity (Table 1). Similarly, all CA variants maintained 100% activity when exposed to a mixture of C_3H_8 (10%) with a balance of CO_2 (90%) or H_2S (0.5%) with a balance of CO_2/N_2 (Table 1). The high activity retention in the presence of C_3H_8 supports our hypothesis that insoluble gases have little to no effect on CA in solution. Retained activity in the presence of H_2S is also consistent with the literature in which CA catalyzed the irreversible cleavage of carbonyl sulfide into H_2S and CO_2.[87]

Considerable changes in CA activity were observed in the presence of NO and SO_2, where ∼100% of the esterase activity was lost in the presence of 1360 and ∼450 ppm of NO and SO_2, respectively (Table 1). This significant loss in activity was observed for all of the CA variants and did not depend on the enzyme's buffer. All of the CA variants retained some level of activity when exposed to lower concentrations of NO (76 ppm) and SO_2 (25 ppm), with the exception of BCA in deionized water, which lost all of its activity even at the lower NO/SO_2 concentration (Table 1). Prior reports suggest that NO can inhibit CA activity when biosynthesized from L-arginine,[88,89] while others reported retained activity of immobilized CA in the presence of NO and SO_2 at levels up to 500 ppm of dry gas.[46,85] Exposure may also result in improved stability in the presence of NO and SO_2. To this point, work by Effendi et al.[56] reported significant improvements in residual CA activity in the presence of HNO_3 and H_2SO_4 for CA immobilized and cross-linked to polymer nanofibers, as compared to free enzyme.

The significant loss of enzymatic activity in the presence of NO and SO_2 may be attributed to changes in pH based on the formation of acids associated with the dissolved gases. The pH of solutions exposed to the different gas mixtures was recorded before and after exposure and is reported in Table 1. Analysis of pH and retained activity suggests that the level of retained activity does not correlate with either the ending pH of the solution or changes in pH following exposure. For example,

https://doi.org/10.1021/acsomega.3c02630
ACS Omega 2023, 8, 37830−37841

Table 1. Enzyme Activity and pH of Bovine Carbonic Anhydrase (BCA) in Deionized Water (DI) or Tris Buffer, Three CA Variants from *Persephonella* (PmCA), and a Proprietary CA (XCA) Exposed to Varying Gas Mixtures for 4 h

enzyme/gas composition[a]	enzyme activity			pH		
	t = 0 h (min^{-1})	t = 4 h (min^{-1})	remaining activity (%)	t = 0 h	t = 4 h	ΔpH
			BCA (DI)			
CO_2	4.8 ± 0.4	5.4 ± 0.4	111 ± 13	9.1	5.4	−3.7
high NO/SO_2	6.0 ± 0.5	0.1 ± 0.0	1 ± 0.1	9.1	3.0	−6.1
low NO/SO_2	3.7 ± 0.3	0.7 ± 0.1	19 ± 2	8.8	4.8	−4.0
H_2S	6.0 ± 0.6	6.6 ± 0.6	110 ± 14	9.0	4.7	−4.3
C_3H_8	4.8 ± 0.2	5.7 ± 0.3	117 ± 9	9.1	4.6	−4.5
			BCA (Tris)			
CO_2	5.6 ± 0.4	5.1 ± 0.4	92 ± 9	7.5	6.4	−1.1
high NO/SO_2	5.7 ± 0.5	0 ± 0	0 ± 0	7.5	5.6	−1.9
low NO/SO_2	4.3 ± 0.3	2.3 ± 0.1	54 ± 4	7.5	5.5	−2.0
H_2S	7.4 ± 0.5	7.3 ± 0.5	100 ± 10	7.5	5.6	−1.9
C_3H_8	5.0 ± 0.4	5.3 ± 0.4	94 ± 4	7.5	5.6	−1.9
			PmCA (WT)			
CO_2	3.5 ± 0.1	3.6 ± 0.1	102 ± 4	7.4	7.0	−0.4
high NO/SO_2	3.9 ± 0.1	0.3 ± 0.1	7 ± 0.6	7.4	6.9	−0.5
low NO/SO_2	2.6 ± 0.1	3.0 ± 0.1	117 ± 7	7.4	6.5	−0.9
H_2S	4.3 ± 0.2	4.3 ± 0.2	100 ± 5	7.4	6.5	−0.9
C_3H_8	4.4 ± 0.1	4.1 ± 0.1	94 ± 4	7.4	6.5	−0.9
			PmCA (WW)			
CO_2	3.0 ± 0.1	3.4 ± 0.1	113 ± 5	7.4	7.0	−0.4
high NO/SO_2	3.5 ± 0.1	0.2 ± 0.1	5 ± 0.3	7.4	6.9	−0.5
low NO/SO_2	1.9 ± 0.1	1.7 ± 0.1	94 ± 3	7.4	6.5	−0.9
H_2S	5.2 ± 0.2	5.3 ± 0.2	101 ± 4	7.4	6.5	−0.9
C_3H_8	4.1 ± 0.1	3.5 ± 0.1	85 ± 3	7.4	6.5	−0.9
			PmCA (SC)			
CO_2	1.8 ± 0.1	1.7 ± 0.1	92 ± 3	7.4	7.0	−0.4
high NO/SO_2	2.4 ± 0.1	0.0 ± 0.0	0 ± 0	7.4	6.9	−0.5
low NO/SO_2	1.4 ± 0.1	1.9 ± 0.1	139 ± 4	7.4	6.5	−0.9
H_2S	2.6 ± 0.1	2.9 ± 0.1	113 ± 3	7.4	6.5	−0.9
C_3H_8	2.2 ± 0.1	2.5 ± 0.1	117 ± 4	7.4	6.5	−0.9
			XCA (Tris)			
CO_2	2.8 ± 0.1	2.8 ± 0.1	100 ± 2	7.5	6.4	−1.1
high NO/SO_2	3.5 ± 0.1	0.2 ± 0.1	6 ± 0.1	7.5	5.6	−1.9
low NO/SO_2	2.3 ± 0.1	1.6 ± 0.1	68 ± 4	7.5	5.5	−2.0
H_2S	1.8 ± 0.1	1.8 ± 0.1	96 ± 4	7.5	5.6	−1.9
C_3H_8	1.8 ± 0.1	1.7 ± 0.1	95 ± 5	7.5	5.6	−1.9

[a]Gas compositions: *CO_2* = 15.3% CO_2, 84.7% N_2; *High NO/SO_2* = 1360 ppm of NO, 454 ppm of SO_2, 15% CO_2, 85% N_2; *Low NO/SO_2* = 75.7 ppm of NO, 25.3 ppm of SO_2, 4.7% N_2, 95.3% CO_2; *H_2S* = 0.5% H_2S,75% CO_2, 24.5% N_2; *C_3H_8* = 10% C_3H_8, 90% CO_2.

BCA in deionized water exhibited ∼20% retention in activity in the presence of low NO and SO_2, and a change in pH of ∼4. In comparison, BCA in deionized water exhibited a 100% retention of activity after exposure to H_2S despite a pH change of 4.3. Therefore, we conclude that the loss of enzyme activity in the presence of NO and SO_2 is not driven solely by associated changes in pH.

3.4. Enzyme Activity, pH, and Conjugate Bases. To better understand the effects of NO and SO_2 on CA activity, a set of experiments was performed to isolate pH and conjugate base effects. NO_x and SO_x readily dissolve into aqueous systems, decomposing to form acids in solution, including HNO_2, HNO_3, H_2SO_3, and H_2SO_4, which have been shown to alter CA activity adversely.[85,90] The esterase activity of BCA and PmCA (WT) was first evaluated in solutions in which a range of acid concentrations, i.e., 1−50 mM HNO_3 or H_2SO_4, were added to the stock enzyme solution.

Considerable losses in esterase activity were observed with as little as 5 mM HNO_3 and 5 mM H_2SO_4 for both BCA and PmCA (Figure 9A). The relative activity continued to decrease as a function of acid concentration, reaching ∼0% residual activity at 50 mM. These results are consistent with those reported previously for the recombinant SyCA (carbonic anhydrase from *Sulfurihydrogenibium yellowstonense*), where the free enzyme lost >80% activity when exposed to 25 mM HNO_3 or H_2SO_4.[56] These results are also consistent with those reported by Bond et al.[84] in which the esterase activity, but not CO_2 hydration activity, was inhibited by NO_3^- and SO_4^{2-}. As noted above, the loss of activity observed in our work may be attributed to decreases in pH associated with the addition of strong acids. At 5 mM HNO_3, the solution of BCA exhibited a pH of 2.4 and residual activity of ∼30%, whereas the solution of PmCA (WT) exhibited a pH of 7 and residual activity of ∼20%. The difference in pH values is attributed to the buffers for BCA (Tris-NaCl) and PmCA (5.5× PBS). Similarly, at 5 mM H_2SO_4, BCA and PmCA (WT) retained ∼20 and 25% activity, respectively, despite significant differences in pH (2.4 for BCA and 6.9 for PmCA). These data suggest that the pH

https://doi.org/10.1021/acsomega.3c02630
ACS Omega 2023, 8, 37830−37841

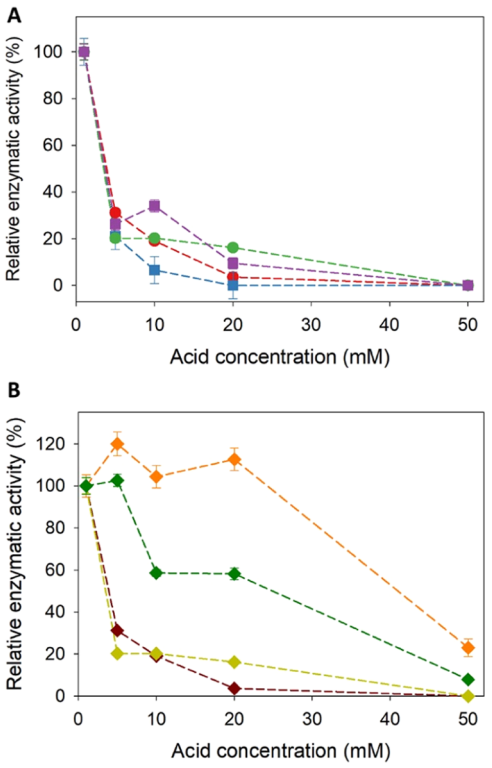

Figure 9. (A) Relative percent activity of BCA exposed to HNO_3 (red -●-) or H_2SO_4 (green -●-) and PmCA (WT) exposed to HNO_3 (blue -■-) or H_2SO_4 (purple -■-). (B) Relative percent activity BCA exposed to HNO_3 (dark red -♦-), HNO_3 with pH adjustment (orange -♦-), H_2SO_4 (yellow green -♦-) or H_2SO_4 with pH adjustment (dark green -♦-). Error bars equal propagated standard error of the mean.

change associated with the addition of HNO_3 and H_2SO_4 is not solely responsible for the observed decrease in activity.

A second set of experiments was performed in which solutions containing 1−50 mM HNO_3 or H_2SO_4 were prepared and the pH was adjusted with the addition of NaOH to achieve a neutral pH (∼7.5). The esterase activity of BCA and PmCA in these buffers was then measured and compared against those in which the pH was not adjusted. Here, BCA in pH-adjusted solutions displayed an enhancement in residual enzyme activity at concentrations ranging from 5 to 20 mM (Figure 9B). At 50 mM, BCA in pH-adjusted solutions retained ∼20 and 8% activity in the presence of HNO_3 and H_2SO_4, respectively. Interestingly, the effect of pH adjustment was less for solutions with H_2SO_4 compared with those with HNO_3, suggesting that the conjugate base may have a direct impact on the enzyme activity. This result is consistent with prior reports of anion species serving as activators and/or inhibitors of CO_2 hydration by CA, where the activation or inhibition was linked to an enhancement or depression in the rate of proton transfer in this reaction.[91] While mechanistically distinct from that of CO_2 hydration, our data suggest that the loss in CA esterase activity in the presence of NO/NO_3 and SO_2/SO_4 may be due to a combination of the conjugate base and the decrease in pH.

4. CONCLUSIONS

Experimental evaluation of CA activity over time at elevated temperatures demonstrates the importance of using stable thermal variants of CA for CO_2 capture applications. Mesostable CAs, such as BCA, display reasonable stability at 4 °C (∼79% over 7 days) but completely lose activity within 3 days at 70 °C. In contrast, thermally stable PmCA variants show a minimal reduction in activity at 4 °C but retain reasonably high activity levels (∼57%) even after 7 days of incubation at 70 °C. Our data also suggest that changes to the electrostatic charge on the outer shell of PmCA do not impact and even may potentially increase the thermal stability of the enzyme. Such changes in the electrostatic shell of the enzyme enable tuning of both the enzyme and support structure (e.g., nanopore) chemistry to optimize CAs as nanoscale functional components of CCS technologies.

Comparative analyses using MD simulations provide insight into the differences in the thermostabilities of BCA and PmCA (WT) at a molecular level. The average global RMSD analysis (entire protein backbone) and average RMSD at a local level (active site residues) show that BCA and PmCA (WT) are relatively stable at the different temperatures tested; however, PmCA shows greater thermostability overall, with average RMSD values less than 0.4 nm for all system temperatures. The PmCA (WT) is considerably more tolerant to high-temperature fluctuations than BCA.

Our secondary structural analysis using DSSP demonstrates minimal loss of α-helicity in PmCA (WT) at all system temperatures except at 140 °C. Interestingly, the BCA sees a significant drop in α-helicity percentage at elevated temperatures (>60 °C). This loss of α-helicity affects CA activity, as evidenced by our esterase assay. The hydrogen bonding analysis supports our observation from the DSSP analysis. While PmCA (WT) only showed a slight decrease in the number of hydrogen bonds at elevated temperatures, the BCA displayed an increased propensity to unfold with the dissociation of hydrogen bonds at a much higher rate. These findings from enzyme structure stability-determining factors, such as RMSD, DSSP, and hydrogen bonding, demonstrate the structural rigidity of PmCA (WT) and its flexibility at the active site to maintain optimal CA activity at extreme temperature conditions compared to BCA.

Contaminating gases can potentially interfere with carbon capture technologies, including hybrid nanoporous CA membranes.[92,93] Here, our data suggest that CA activity is robust against contaminating gases, including H_2S and propane, and industrially relevant concentrations of NO and SO_2. With respect to the latter, loss of activity was observed in the presence of high concentrations of NO and SO_2, but the system displayed high levels of activity retention at lower concentrations that are more applicable to industrial effluents. While the exposure of CA solutions to the different gases induced considerable changes in pH, these changes were not strongly correlated to the change in CA activity.

Further investigation suggested that the loss of CA activity in the presence of NO and SO_2 is likely due to inhibition by the conjugate base and changes in pH. Specifically, we demonstrated that CA activity could be retained by adjusting the pH to neutral while maintaining various levels of NO_3^- and SO_4^{2-}. This observation is critical to selecting a proper solution buffer to mitigate drastic changes in pH observed in deionized water compared with smaller changes observed with 5.5× PBS. A dose-dependent correlation between activity loss and NO_3^-/SO_4^{2-} concentration was also observed in these data, suggesting that the conjugate base maintains some interaction with CA, causing inhibition or loss in activity. Significant activity loss was observed at high concentrations, while lower and more application-relevant concentrations of NO_3^-/SO_4^{2-}

https://doi.org/10.1021/acsomega.3c02630
ACS Omega 2023, 8, 37830−37841

had a minimal effect on enzyme activity. It should be noted that our data were based on the esterase activity of CA, which has been shown to be more sensitive than CO_2 hydration activity to NO_3^- and SO_4^{2-}.[84] As such, the minimal effects of contaminating gases on the activity of BCA and PmCA support their use in carbon capture applications.

Our data provide a baseline assessment of CA activity under conditions relevant to carbon capture applications. A critical next step involves a similar characterization of hybrid membranes in which CA is used for CO_2 capture and release. The superior stability against high temperatures and contaminating gases makes the PmCA variant an attractive candidate for evaluation. Related work in this area suggests that confinement in nanoporous matrices has the potential to surface-enhance this stability and provide a path forward to realizing the commercial application of this technology.[31]

AUTHOR INFORMATION

Corresponding Authors

Susan B. Rempe − *Center for Integrated Nanotechnologies, Sandia National Laboratories, Albuquerque, New Mexico 87185, United States;* orcid.org/0000-0003-1623-2108; Email: slrempe@sandia.gov

George D. Bachand − *Center for Integrated Nanotechnologies, Sandia National Laboratories, Albuquerque, New Mexico 87185, United States;* orcid.org/0000-0002-3169-9980; Email: gdbacha@sandia.gov

Authors

Arjun Sharma − *Department of Physics, The University of Vermont, Burlington, Vermont 05405-0160, United States;* Present Address: Department of Chemistry and Biochemistry, Purdue University Fort Wayne, Fort Wayne, Indiana 46805, United States

Rong-an Chiang − *Memzyme, LLC, Albuquerque, New Mexico 87123, United States*

Monica Manginell − *Center for Integrated Nanotechnologies, Sandia National Laboratories, Albuquerque, New Mexico 87185, United States*

Isaac Nardi − *Epigentor Consultants, Inc., Miami, Florida 87185, United States*

Eric N. Coker − *Electronic, Optical, and Nanomaterials Department, Sandia National Laboratories, Albuquerque, New Mexico 87185, United States;* orcid.org/0000-0002-9382-9373

Juan M. Vanegas − *Department of Physics, The University of Vermont, Burlington, Vermont 05405-0160, United States;* orcid.org/0000-0003-1381-1649

Complete contact information is available at: https://pubs.acs.org/10.1021/acsomega.3c02630

Author Contributions

#A.S. and R-a.C. contributed equally to this work.

Notes

The authors declare no competing financial interest.

ACKNOWLEDGMENTS

The authors thank the Laboratory Research and Development (LDRD) Program at Sandia National Laboratories for support. This work was performed, in part, at the Center for Integrated Nanotechnologies, an Office of Science User Facility operated for the U.S. Department of Energy (DOE) Office of Science. Computations were performed, in part, on the Vermont Advanced Computing Core supported in part by NSF Award No. OAC-1827314. This article has been authored by employees of National Technology & Engineering Solutions of Sandia, LLC under Contract No. DE-NA0003525 with the U.S. Department of Energy (DOE). The employee owns all right, title, and interest in and to the article and is solely responsible for its contents. The United States Government retains and the publisher, by accepting the article for publication, acknowledges that the United States Government retains a nonexclusive, paid-up, irrevocable, worldwide license to publish or reproduce the published form of this article or allow others to do so, for United States Government purposes. The DOE will provide public access to these results of federally sponsored research in accordance with the DOE Public Access Plan https://www.energy.gov/downloads/doe-public-access-plan.

REFERENCES

(1) Forster PR, V.; Artaxo, P.; Berntsen, T.; Betts, R.; Fahey, D. W.; Haywood, J.; Lean, J.; Lowe, D. C.; Myhre, G.; Nganga, J.; Prinn, R.; Raga, G.; Schultz, M.; Van Dorland, R. *Changes in Atmospheric Constituents and In Radiative Forcing*; Cambridge University Press: Cambridge, United Kingdom, 2007.

(2) WMO Greenhouse Gas Bulletin. The State of Greenhouse Gases in the Atmosphere Based on Global Observations through 2020. [updated October 25, 2021]. https://library.wmo.int/doc_num.php?explnum_id=10904.

(3) International Energy Agency. Global Energy Review, Paris, France. 2021. https://www.iea.org/reports/global-energy-review-2021.

(4) Weart, S. The Carbon Dioxide Greenhouse Effect: American Institute of Physics, 2008. https://history.aip.org/climate/co2.htm.

(5) Spahni, R.; Chappellaz, J.; Stocker, T. F.; Loulergue, L.; Hausammann, G.; Kawamura, K.; et al. Atmospheric methane and nitrous oxide of the Late Pleistocene from Antarctic ice cores. *Science* **2005**, *310* (5752), 1317−1321.

(6) Siegenthaler, U.; Stocker, T. F.; Monnin, E.; Luthi, D.; Schwander, J.; Stauffer, B.; et al. Stable carbon cycle-climate relationship during the late Pleistocene. *Science* **2005**, *310* (5752), 1313−1317.

(7) Petit, J. R.; Jouzel, J.; Raynaud, D.; Barkov, N. I.; Barnola, J. M.; Basile, I.; et al. Climate and atmospheric history of the past 420,000 years from the Vostok ice core, Antarctica. *Nature* **1999**, *399* (6735), 429−436.

(8) Houghton, J. T.; Ding, Y.; Griggs, D. J. et al. Climate Change 2001: The Scientific Basis. Cambridge, UK, 2001, https://pure.mpg.de/rest/items/item_995493/component/file_995492/content.

(9) International Energy Agency. 20 years of carbon capture and storage Paris, France. https://www.iea.org/reports/20-years-of-carbon-capture-and-storage.

(10) Ferron, P. *Absorption-Based Post-Combustion Capture of Carbon Dioxide*, 1st ed.; Woodhead Publishing, 2016.

(11) Vaidya, P. D.; Kenig, E. Y. CO_2-alkanolamine reaction kinetics: A review of recent studies. *Chem. Eng. Technol.* **2007**, *30* (11), 1467−1474.

(12) Rubin, E. S.; Davison, J. E.; Herzog, H. J. The cost of CO_2 capture and storage. *Int. J. Greenhouse Gas Control* **2015**, *40*, 378−400.

(13) Fradette, L.; Lefebvre, S.; Carley, J. Demonstration Results of Enzyme-Accelerated CO_2 Capture. *Energy Procedia.* **2017**, *114*, 1100−1109.

(14) Favre, E. Membrane processes and postcombustion carbon dioxide capture: Challenges and prospects. *Chem. Eng. J.* **2011**, *171* (3), 782−793.

https://doi.org/10.1021/acsomega.3c02630
ACS Omega 2023, 8, 37830−37841

(15) Merkel, T. C.; Lin, H. Q.; Wei, X. T.; Baker, R. Power plant post-combustion carbon dioxide capture: An opportunity for membranes. *J. Membr. Sci.* **2010**, *359* (1−2), 126−139.
(16) Baker, R. W.; Low, B. T. Gas Separation Membrane Materials: A Perspective. *Macromolecules* **2014**, *47* (20), 6999−7013.
(17) Favre, E. Membrane Separation Processes and Post-Combustion Carbon Capture: State of the Art and Prospects. *Membranes* **2022**, *12* (9), No. 884.
(18) Ramasubramanian, K.; Ho, W. S. W. Recent developments on membranes for post-combustion carbon capture. *Curr. Opin Chem. Eng.* **2011**, *1* (1), 47−54.
(19) He, X. A review of material development in the field of carbon capture and the application of membrane-based processes in power plants and energy-intensive industries. *Energy Sustainable Soc.* **2018**, *8*, No. 34, DOI: 10.1186/s13705-018-0177-9.
(20) Xu, J.; Wang, Z.; Qiao, Z.; Wu, H.; Dong, S.; Zhao, S.; Wang, J. Post-combustion CO_2 capture with membrane process: Practical membrane performance and appropriate pressure. *J. Membr. Sci.* **2019**, *581*, 195−213.
(21) Alqaheem, Y.; Alomair, A.; Vinoba, M.; Pérez, A. Polymeric Gas-Separation Membranes for Petroleum Refining. *Int. J. Polym. Sci.* **2017**, *2017*, No. 4250927.
(22) Li, Q.; Wu, H.; Wang, Z.; Wang, J. Analysis and optimal design of membrane processes for flue gas CO_2 capture. *Sep. Purif. Technol.* **2022**, *298*, No. 121584.
(23) Khalilpour, R.; Mumford, K.; Zhai, H.; Abbas, A.; Stevens, G.; Rubin, E. S. Membrane-based carbon capture from flue gas: a review. *J. Cleaner Prod.* **2015**, *103*, 286−300.
(24) Ziobrowski, Z.; Rotkegel, A. Comparison of CO_2 Separation Efficiency from Flue Gases Based on Commonly Used Methods and Materials. *Materials* **2022**, *15* (2), No. 460.
(25) Merkel, T.; Amo, K.; Baker, R.; Daniels, R.; Friat, B.; He, Z. et al. *Membrane Process to Sequester CO_2 From Power Plant Flue Gas*; Membrane Technology & Research Incorporated, 2009.
(26) Zhao, M.; Yang, Y.; Xue-Song, G. MOF based CO_2 capture: Adsorption and membrane separation. *Inorg. Chem. Commun.* **2023**, *152*, No. 110722.
(27) Olabi, A. G.; Alami, A. H.; Ayoub, M.; Aljaghoub, H.; Alasad, S.; Inayat, A.; et al. Membrane-based carbon capture: Recent progress, challenges, and their role in achieving the sustainable development goals. *Chemosphere* **2023**, *320*, No. 137996.
(28) Yong, J. K. J.; Stevens, G. W.; Caruso, F.; Kentish, S. E. In situ layer-by-layer assembled carbonic anhydrase-coated hollow fiber membrane contactor for rapid CO_2 absorption. *J. Membr. Sci.* **2016**, *514*, 556−565.
(29) Hou, J. W.; Zulkifli, M. Y.; Mohammad, M.; Zhang, Y. T.; Razmjou, A.; Chen, V. Biocatalytic gas-liquid membrane contactors for CO_2 hydration with immobilized carbonic anhydrase. *J. Membr. Sci.* **2016**, *520*, 303−313.
(30) Abdelrahim, M. Y. M.; Neves, LA.; Capasso, C. S. C.; Coelhoso, I. M.; Crespo, J. G.; Barboiu, M.; et al. Supported ionic liquid membranes immobilized with carbonic anhydrases for CO_2 transport at high temperatures. *J. Membr. Sci.* **2017**, *528*, 225−230.
(31) Fu, Y. Q.; Jiang, Y. B.; Dunphy, D.; Xiong, H. F.; Coker, E.; Chou, S.; et al. Ultra-thin enzymatic liquid membrane for CO_2 separation and capture. *Nat. Commun.* **2018**, *9*, No. 990.
(32) Aggarwal, M.; Boone, C. D.; Kondeti, B.; McKenna, R. Structural annotation of human carbonic anhydrases. *J. Enzyme Inhib. Med. Chem.* **2013**, *28* (2), 267−277.
(33) Krishnamurthy, V. M.; Kaufman, G. K.; Urbach, A. R.; Gitlin, I.; Gudiksen, K. L.; Weibel, D. B.; Whitesides, G. M. Carbonic anhydrase as a model for biophysical and physical-organic studies of proteins and protein-ligand binding. *Chem. Rev.* **2008**, *108* (3), 946−1051.
(34) Lindskog, S. Structure and mechanism of carbonic anhydrase. *Pharmacol. Therapeut.* **1997**, *74* (1), 1−20.
(35) Xu, Y.; Lin, Y.; Chew, N. G. P.; Malde, C.; Wang, R. Biocatalytic PVDF composite hollow fiber membranes for CO_2 removal in gas-liquid membrane contactor. *J. Membr. Sci.* **2019**, *572*, 532−544.
(36) Jiao, D.; Rempe, S. B. Combined density functional theory (DFT) and continuum calculations of pKa in carbonic anhydrase. *Biochemistry* **2012**, *51* (30), 5979−5989.
(37) Jiao, D.; Rempe, S. B. CO_2 solvation free energy using quasi-chemical theory. *J. Chem. Phys.* **2011**, *134* (22), No. 224506.
(38) Drozdov, A. S.; Shapovalova, O. E.; Ivanovski, V.; Avnir, D.; Vinogradov, V. V. Entrapment of Enzymes within Sol-Gel-Derived Magnetite. *Chem. Mater.* **2016**, *28* (7), 2248−2253.
(39) Chen, X. X.; Wang, Y. B.; Wang, P. Peptide-Induced Affinity Binding of Carbonic Anhydrase to Carbon Nanotubes. *Langmuir* **2015**, *31* (1), 397−403.
(40) Yu, Y. H.; Chen, B. W.; Qi, W.; Li, X. L.; Shin, Y.; Lei, C. H.; Liu, J. Enzymatic conversion of CO_2 to bicarbonate in functionalized mesoporous silica. *Microporous Mesoporous Mater.* **2012**, *153*, 166−170.
(41) Hou, J. W.; Dong, G. X.; Xiao, B. W.; Malassigne, C.; Chen, V. Preparation of titania based biocatalytic nanoparticles and membranes for CO_2 conversion. *J. Mater. Chem. A* **2015**, *3* (7), 3332−3342.
(42) Karlsson, M.; Carlsson, U. Protein adsorption orientation in the light of fluorescent probes: Mapping of the interaction between site-directly labeled human carbonic anhydrase II and silica nanoparticles. *Biophys. J.* **2005**, *88* (5), 3536−3544.
(43) Zhang, Y. Z. J.; Zhu, J.; Hou, J.; Hou, J.; Yi, S.; Yi, S.; Bruggen, B. V. D.; Van der Bruggen, B.; Zhan, Y. Carbonic anhydrase membranes for carbon capture and storage. *J. Membr. Sci. Lett.*. **2022**, *2* (2), No. 100031.
(44) Kanbar, B.; Ozdemir, E. Thermal stability of carbonic anhydrase immobilized within polyurethane foam. *Biotechnol. Prog.* **2010**, *26* (5), 1474−1480.
(45) Sun, H.; Han, J. H.; Han, J.; Jo, Y. W.; Jo, Y.; Han, S. O.; Han, S. O.; Hyeon, J. E.; Hyeon, J. E. Increased thermal stability of the carbonic anhydrase enzyme complex for the efficient reduction of CO_2 through cyclization and polymerization by peptide bonding. *Process Biochem.* **2022**, *120*, 195−201.
(46) Molina-Fernández, C.; Luis, P. Immobilization of carbonic anhydrase for CO_2 capture and its industrial implementation: A review. *J. CO_2 Util.* **2021**, *47*, No. 101475.
(47) Faridi, S.; Satyanarayana, T. Novel alkalistable alpha-carbonic anhydrase from the polyextremophilic bacterium Bacillus halodurans: characteristics and applicability in flue gas CO_2 sequestration. *Environ. Sci. Pollut. Res. Int.* **2016**, *23* (15), 15236−15249.
(48) Borchert, M. S. Novozymes. Heat-Stable Persephonella Carbonic Anhydrases. U.S. patent US9909115, 2018.
(49) Capasso, C.; De Luca, V.; Carginale, V.; Cannio, R.; Rossi, M. Biochemical properties of a novel and highly thermostable bacterial alpha-carbonic anhydrase from *Sulfurihydrogenibium yellowstonense* YO3AOP1. *J. Enzym. Inhib. Med. Chem.* **2012**, *27* (6), 892−897.
(50) De Luca, V. D.; Vullo, D.; Scozzafava, A.; Carginale, V.; Rossi, M.; Supuran, C. T.; Capasso, C. An α-carbonic anhydrase from the thermophilic bacterium Sulphurihydrogenibium azorense is the fastest enzyme known for the CO_2 hydration reaction. *Bioorg. Med. Chem.* **2013**, *21* (21), 1465−1469.
(51) Andersen, J. L.; Schroder, T. J.; Christensen, S.; Strandbygard, D.; Pallesen, L. T.; Garcia-Alai, M. M.; et al. Identification of the first small-molecule ligand of the neuronal receptor sortilin and structure determination of the receptor-ligand complex. *Acta Crystallogr., Sect. D: Struct. Biol.* **2014**, *70* (Pt 2), 451−460.
(52) Kanth, B. K.; Jun, S. Y.; Kumari, S.; Pack, S. P. Highly thermostable carbonic anhydrase from *Persephonella marina* EX-H1: Its expression and characterization for CO_2-sequestration applications. *Process Biochem.* **2014**, *49* (12), 2114−2121.
(53) Cha, H. J.; Jo, B. H.; Seo, J. H.; Posttech Academy-Industry Foundation. Carbonic anhydrase having high-temperature stability and carbon dioxide collector comprising same. WO2015/056858 A1, 2025.

https://doi.org/10.1021/acsomega.3c02630
ACS Omega 2023, 8, 37830−37841

(54) Steger, F.; Reich, J.; Fuchs, W.; Rittmann, S.; Gübitz, G. M.; Guebitz, G. M.; Ribitsch, D. Comparison of Carbonic Anhydrases for CO_2 Sequestration. *Int. J. Mol. Sci.* **2022**, *23* (2), No. 957.
(55) Jo, B. H.; Seo, J. H.; Cha, H. J. Bacterial extremo-α-carbonic anhydrases from deep-sea hydrothermal vents as potential biocatalysts for CO_2 sequestration. *J. Mol. Catal. B: Enzym.* **2014**, *109*, 31−39.
(56) Effendi, S. S. W.; Chiu, C.-Y.; Chang, Y.-K.; Ng, I.-S. Crosslinked on novel nanofibers with thermophilic carbonic anhydrase for carbon dioxide sequestration. *Int. J. Biol. Macromol.* **2020**, *152*, 930−938.
(57) Wu, X. Z. Q.; Zhang, L.; Zhang, L.; Liu, S.; Liu, S.; Chen, G.; Chen, G.; Zhang, H.; Zhang, H.; Wang, L. Insights Into the Role of Exposed Surface Charged Residues in the Alkali-Tolerance of GH11 Xylanase. *Front Microbiol.* **2020**, *11*, No. 837.
(58) Shaw, K. L.; Grimsley, G. R.; Yakovlev, G. I.; Makarov, A. A.; Pace, C. N. The effect of net charge on the solubility, activity, and stability of ribonuclease Sa. *Protein Sci.* **2001**, *10* (6), 1206−1215.
(59) Mikulski, R.; West, D.; Sippel, K. H.; Avvaru, B. S.; Aggarwal, M.; Tu, C.; et al. Water networks in fast proton transfer during catalysis by human carbonic anhydrase II. *Biochemistry* **2013**, *52* (1), 125−131.
(60) Maupin, C. M.; Voth, G. A. Proton transport in carbonic anhydrase: Insights from molecular simulation. *Biochim. Biophys. Acta, Proteins Proteomics* **2010**, *1804* (2), 332−341.
(61) Kim, C. U.; Song, H.; Avvaru, B. S.; Gruner, S. M.; Park, S.; McKenna, R. Tracking solvent and protein movement during CO_2 release in carbonic anhydrase II crystals. *Proc. Natl. Acad. Sci. U.S.A.* **2016**, *113* (19), 5257−5262.
(62) Angeli, A.; Carta, F.; Supuran, C. T. Carbonic Anhydrases: Versatile and Useful Biocatalysts in Chemistry and Biochemistry. *Catalysts* **2020**, *10* (9), No. 1008.
(63) Jo, B. H.; Seo, J. H.; Cha, H. J. Bacterial extremo-alpha-carbonic anhydrases from deep-sea hydrothermal vents as potential biocatalysts for CO_2 sequestration. *J. Mol. Catal. B: Enzym.* **2014**, *109*, 31−39.
(64) Uda, N. R.; Seibert, V.; Stenner-Liewen, F.; Müller, P.; Herzig, P.; Gondi, G.; et al. Esterase activity of carbonic anhydrases serves as surrogate for selecting antibodies blocking hydratase activity. *J. Enzym. Inhib. Med. Chem.* **2015**, *30* (6), 955−960.
(65) Abraham, M. J.; Murtola, T.; Schulz, R.; Páll, S.; Smith, J. C.; Hess, B.; Lindahl, E. GROMACS: High performance molecular simulations through multi-level parallelism from laptops to supercomputers. *SoftwareX* **2015**, *1−2*, 19−25.
(66) Macchiagodena, M.; Pagliai, M.; Andreini, C.; Rosato, A.; Procacci, P. Upgrading and Validation of the AMBER Force Field for Histidine and Cysteine Zinc(II)-Binding Residues in Sites with Four Protein Ligands. *J. Chem. Inf Model.* **2019**, *59* (9), 3803−3816.
(67) Macchiagodena, M.; Pagliai, M.; Andreini, C.; Rosato, A.; Procacci, P. Upgraded AMBER Force Field for Zinc-Binding Residues and Ligands for Predicting Structural Properties and Binding Affinities in Zinc-Proteins. *ACS Omega* **2020**, *5* (25), 15301−15310.
(68) Hornak, V.; Abel, R.; Okur, A.; Strockbine, B.; Roitberg, A.; Simmerling, C. Comparison of multiple amber force fields and development of improved protein backbone parameters. *Proteins* **2006**, *65* (3), 712−725.
(69) Lindorff-Larsen, K.; Piana, S.; Palmo, K.; Maragakis, P.; Klepeis, J. L.; Dror, R. O.; Shaw, D. E. Improved side-chain torsion potentials for the Amber ff99SB protein force field. *Proteins* **2010**, *78* (8), 1950−1958.
(70) Jorgensen, W. L.; Chandrasekhar, J.; Madura, J. D.; Impey, R. W.; Klein, M. L. Comparison of Simple Potential Functions for Simulating Liquid Water. *J. Chem. Phys.* **1983**, *79* (2), 926−935.
(71) Olsson, M. H. M.; Sondergaard, C. R.; Rostkowski, M.; Jensen, J. H. PROPKA3: Consistent Treatment of Internal and Surface Residues in Empirical pKa Predictions. *J. Chem. Theory Comput.* **2011**, *7* (2), 525−537.
(72) Søndergaard, C. R.; Olsson, M. H.; Rostkowski, M.; Jensen, J. H. Improved Treatment of Ligands and Coupling Effects in Empirical Calculation and Rationalization of pKa Values. *J. Chem. Theory Comput.* **2011**, *7* (7), 2284−2295.
(73) Petersen, H. G. Accuracy and Efficiency of the Particle Mesh Ewald Method. *J. Chem. Phys.* **1995**, *103* (9), 3668−3679.
(74) Hess, B.; Bekker, H.; Berendsen, H. J. C.; Fraaije, JGEM. LINCS: A linear constraint solver for molecular simulations. *J. Comput. Chem.* **1997**, *18* (12), 1463−1472.
(75) Bussi, G. D. D.; Donadio, D.; Parrinello, M. Canonical sampling through velocity rescaling. *J. Chem. Phys.* **2007**, *126* (1), No. 014101.
(76) Bernetti, M. B. G.; Bussi, G. Pressure control using stochastic cell rescaling. *J. Chem. Phys.* **2020**, *153* (11), No. 114107.
(77) Pettersen, E. F.; Goddard, T. D.; Huang, C. C.; Couch, G. S.; Greenblatt, D. M.; Meng, E. C.; Ferrin, T. E. UCSF chimera - A visualization system for exploratory research and analysis. *J. Comput. Chem.* **2004**, *25* (13), 1605−1612.
(78) Humphrey, W.; Dalke, A.; Schulten, K. VMD: Visual molecular dynamics. *J. Mol. Graphics Modell.* **1996**, *14* (1), 33−38.
(79) Kabsch, W.; Sander, C. Dictionary of Protein Secondary Structure - Pattern-Recognition of Hydrogen-Bonded and Geometrical Features. *Biopolymers.* **1983**, *22* (12), 2577−2637.
(80) Bose, H.; Satyanarayana, T. Microbial Carbonic Anhydrases in Biomimetic Carbon Sequestration for Mitigating Global Warming: Prospects and Perspectives. *Front Microbiol.* **2017**, *8*, No. 1615.
(81) Demir, Y.; Demir, N.; Nadaroglu, H.; Bakan, E. Purification and characterization of carbonic anhydrase from bovine erythrocyte plasma membrane. *Prep. Biochem. Biotechnol.* **2000**, *30* (1), 49−59.
(82) Alaei, L.; Moosavi-Movahedi, A. A.; Hadi, H.; Saboury, A. A.; Ahmad, F.; Amani, M. Thermal inactivation and conformational lock of bovine carbonic anhydrase. *Protein Pept. Lett.* **2012**, *19* (8), 852−858.
(83) Sarraf, N. S.; Saboury, A. A.; Ranjbar, B.; Moosavi-Movahedi, A. A. Structural and functional changes of bovine carbonic anhydrase as a consequence of temperature. *Acta Biochim. Pol.* **2004**, *51* (3), 665−671.
(84) Bond, G. M.; Stringer, J.; Brandvold, D. K.; Simsek, F. A.; Medina, M.-G.; Egeland, G. Development of integrated system for biomimetic CO_2 sequestration using the enzyme carbonic anhydrase. *Energy Fuels* **2001**, *15* (2), 309−316.
(85) Yong, J. K. J.; Stevens, G. W.; Caruso, F.; Kentish, S. E. The resilience of carbonic anhydrase enzyme for membrane-based carbon capture applications. *Int. J. Greenhouse Gas Control* **2017**, *62*, 122−129.
(86) Bing, L.; Yongqiang, S.; Qilong, Z.; Can, Z.; Haoran, D. Pollutants emission characteristics of an ultra-low coal-fired power unit. *IOP Conf. Ser.: Earth Environ. Sci.* **2018**, *159*, No. 012014.
(87) Protoschill-Krebs, G.; Wilhelm, C.; Kesselmeier, J. Consumption of carbonyl sulphide (COS) by higher plant carbonic anhydrase (CA). *Atmos. Environ.* **1996**, *30* (18), 3151−3156.
(88) Puscas, I.; Coltau, M. Inhibition of carbonic anhydrase by nitric oxide. *Arzneimittelforschung* **1995**, *45* (8), 846−848.
(89) Puscas, I.; Coltau, M.; Domuta, G.; Baican, M.; Puscas, C.; Pasca, R. Carbonic Anhydrase I Inhibition By Nitric Oxide: Implications For Mediation Of The Hypercapnia-Induced Vasodilator Response. *Clin. Exp. Pharmacol. Physiol.* **2000**, *27* (1−2), 95−99.
(90) Bertucci, A.; Innocenti, A.; Zoccola, D.; Scozzafava, A.; Allemand, D.; Tambutte, S.; Supuran, C. T. Carbonic anhydrase inhibitors: inhibition studies of a coral secretory isoform with inorganic anions. *Bioorg. Med. Chem. Lett.* **2009**, *19* (3), 650−653.
(91) Rowlett, R. S.; Gargiulo, N. J., 3rd; Santoli, F. A.; Jackson, J. M.; Corbett, A. H. Activation and inhibition of bovine carbonic anhydrase III by dianions. *J. Biol. Chem.* **1991**, *266* (2), 933−941.
(92) He, X.; Hägg, M. B. Hollow fiber carbon membranes: From material to application. *Chem. Eng. J.* **2013**, *215−216*, 440−448.
(93) Kárászová, M. Z. B.; Petrusová, Z.; Červenka, V.; Bobák, M.; Šyc, M.; Izák, P. Post-combustion carbon capture by membrane separation, Review. *Sep. Purif. Technol.* **2020**, *238*, No. 116448.

NOTE ADDED AFTER ASAP PUBLICATION

Changes to the captions of Figures 3 and 9 were published on October 17, 2023.

https://doi.org/10.1021/acsomega.3c02630
ACS Omega 2023, 8, 37830−37841